




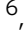





# New signatures of the spin gap in quantum point contacts

K. L. Hudson <sup>1,2</sup>, A. Srinivasan<sup>1,2</sup>, O. Goulko <sup>3</sup>, J. Adam<sup>1</sup>, Q. Wang <sup>1,2</sup>, L. A. Yeoh<sup>1</sup>, O. Klochan<sup>1,2</sup>, I. Farrer <sup>4</sup>, D. A. Ritchie <sup>5</sup>, A. Ludwig <sup>6</sup>, A. D. Wieck <sup>6</sup>, J. von Delft <sup>7</sup> & A. R. Hamilton <sup>1,2</sup>✉

One dimensional semiconductor systems with strong spin-orbit interaction are both of fundamental interest and have potential applications to topological quantum computing. Applying a magnetic field can open a spin gap, a pre-requisite for Majorana zero modes. The spin gap is predicted to manifest as a field dependent dip on the first 1D conductance plateau. However, disorder and interaction effects make identifying spin gap signatures challenging. Here we study experimentally and numerically the 1D channel in a series of low disorder p-type GaAs quantum point contacts, where spin-orbit and hole-hole interactions are strong. We demonstrate an alternative signature for probing spin gaps, which is insensitive to disorder, based on the linear and non-linear response to the orientation of the applied magnetic field, and extract a spin-orbit gap  $\Delta E \approx 500 \mu\text{eV}$ . This approach could enable one-dimensional hole systems to be developed as a scalable and reproducible platform for topological quantum applications.

<sup>1</sup>School of Physics, University of New South Wales, Sydney, NSW 2052, Australia. <sup>2</sup>ARC Centre of Excellence in Future Low-Energy Electronics Technologies, University of New South Wales, Sydney, NSW 2052, Australia. <sup>3</sup>Department of Physics, University of Massachusetts, Boston, MA 02125, USA. <sup>4</sup>Cavendish Laboratory, University of Cambridge, Madingley Road, Cambridge, UK. <sup>5</sup>Department of Electronic and Electrical Engineering, University of Sheffield, Sheffield, UK. <sup>6</sup>Angewandte Festkörperphysik, Ruhr-Universität Bochum, D-44780 Bochum, Germany. <sup>7</sup>Arnold Sommerfeld Center for Theoretical Physics, Ludwig-Maximilians Universität, München, Theresienstrasse 37, D-80333 München, Germany. ✉email: [alex.hamilton@unsw.edu.au](mailto:alex.hamilton@unsw.edu.au)

The physics of 1D (one-dimensional) electron and hole systems has been an area of ongoing research interest since conductance quantised in integer multiples of  $2e^2/h$  was discovered in short quantum point contacts (QPCs) in GaAs heterostructures<sup>1,2</sup>. The Landauer–Büttiker formalism describes the quantised steps in ballistic 1D conductance by means of transmission probabilities<sup>3</sup>. In QPCs in the quantum limit, many-body interactions lead to an additional anomalous feature below the first conductance plateau at  $0.7 \times 2e^2/h$ <sup>4,5</sup>. In longer 1D systems, interaction-driven spin–charge separation (where spin and charge excitations travel at different speeds through the 1D constriction) has also been observed<sup>6,7</sup>.

Recently, there has been a resurgence of interest in 1D systems with strong spin–orbit interaction (SOI) due to the potential for engineering non-trivial topological superconductivity. A semi-conducting quantum wire with strong SOI can host p-wave superconductivity and Majorana zero-mode states when coupled to a regular s-wave superconductor<sup>8–10</sup>. The system is tuned from the trivial to the topological regime by the application of a magnetic field perpendicular to the effective spin–orbit field  $\mathbf{B}_{\text{SOI}}$  in the wire. This mixes the two chiral spin species, opening up a spin gap at  $\mathbf{k} = 0$ . When the Fermi energy  $E_F$  is tuned into this spin gap, the states at  $E_F$  effectively become spinless and Majorana zero modes can form at the ends of the wire.

The key experimental signature of the opening of a spin gap in a quantum wire or point contact with normal contacts is the appearance of a ‘dip’ in conductance on the first 1D subband plateau when a magnetic field is applied parallel to the current direction<sup>11–13</sup>. However, electron–electron interaction effects become strong in the 1D limit, increasing the magnetic susceptibility and spin gap. These interactions cause additional conductance features near  $0.7 \times 2e^2/h$  that change the spin-gap signatures predicted by single-particle models. Furthermore, unambiguous identification of this spin gap dip is complicated by disorder and finite-length effects in the 1D channel which can also cause dips and oscillations on the first conductance plateau<sup>13–15</sup>. To overcome these complications the 1D system should be free of unwanted disorder and non-adiabatic effects, and the analysis should include many-body interactions.

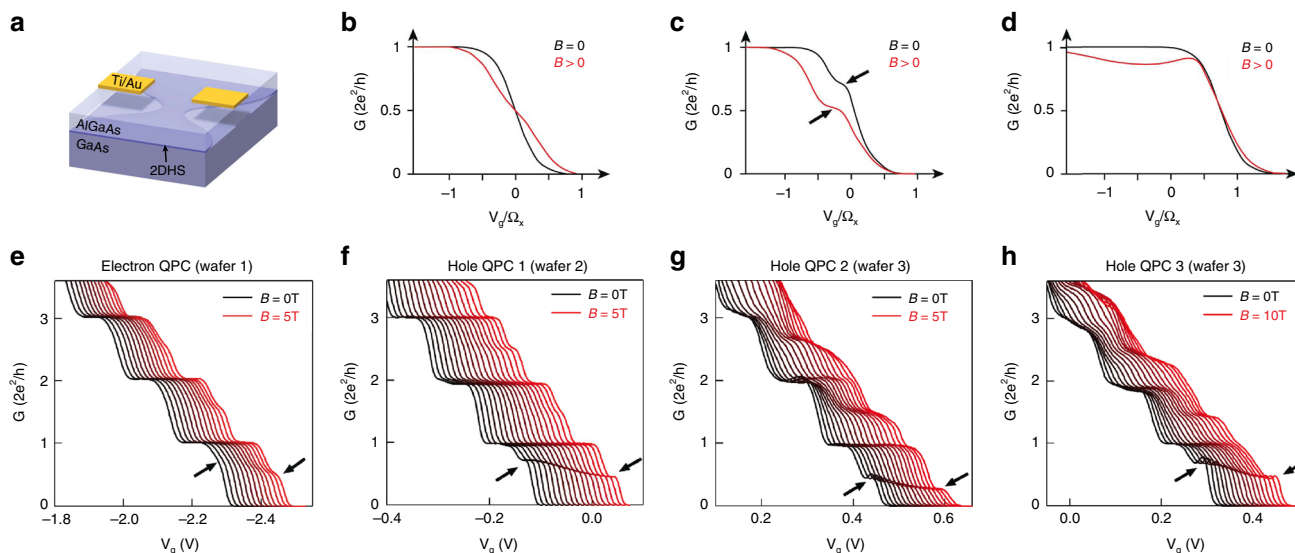
In this study, we examine the 0.7 anomaly and spin-gap signatures in ultra-low disorder, adiabatic QPCs on GaAs using both electrons (no SOI) and holes (strong SOI). In III-V and group IV semiconductors the conduction band electrons originate from  $l = 0$  s-shell atomic orbitals, so have weak  $l$  s SOIs (where  $s = \pm \frac{1}{2}$  is the electron spin). Valence band holes are formed from  $l = 1$  p-shell orbitals, so have strong spin–orbit coupling and a total angular momentum  $J = L + S = \pm \frac{3}{2}$ . The 2D quantum well confinement causes a splitting of the  $m_j = \pm \frac{1}{2}$  light-hole and  $m_j = \pm \frac{3}{2}$  heavy-hole bands at  $\mathbf{k} = 0$  of order  $\sim 10$  meV, so that only the heavy hole states are occupied<sup>16</sup>. For both electrons and holes, a magnetic field parallel to the current causes Zeeman splitting of the higher subbands, and a characteristic evolution of the 0.7 anomaly to  $0.5 \times 2e^2/h$  in magnetic field. However, for holes we find that while the evolution of the conductance is not affected by the strong SOI, the opening of a spin gap shifts the 0.7 anomaly in energy and causes the apparent  $g$ -factor of the first 1D subband to go to zero. Our results are explained by numerical functional renormalisation group calculations of a tight-binding model that accounts for spin–orbit and strong electron–electron interactions on an equal footing<sup>17</sup> and we extract a spin–orbit gap  $\Delta E \approx 500 \mu\text{eV}$  for hole QPCs. Most significantly, we show that rotating the in-plane magnetic field so that it is parallel or perpendicular to the spin–orbit field inside the QPC opens and closes the spin gap, and produces a unique signature of the spin gap in the magnetoconductance.

## Results

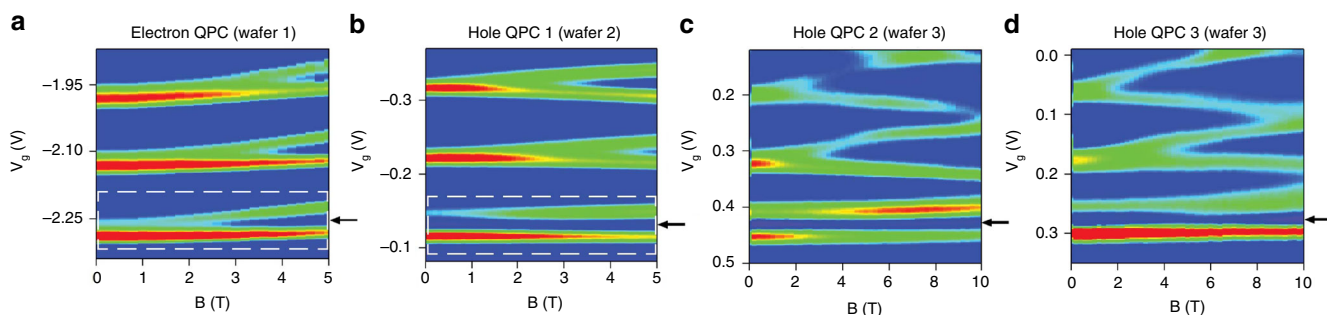
Figure 1a is a schematic of a typical QPC device (dimensions of all devices are given in Supplementary Table 1). The 2D systems have typical mean free paths of  $5 \mu\text{m}$  for both electrons and holes, and carrier densities of  $1.5\text{--}2.5 \times 10^{11} \text{ cm}^{-2}$ . Figure 1b–d shows schematically how the conductance of a QPC with a saddle point potential  $V = V_0 - \frac{1}{2}m\omega_x^2x^2 + \frac{1}{2}m\omega_y^2y^2$  depends on the applied magnetic field  $\mathbf{B}$  (the magnetic field axes are scaled with  $\Omega_x$ , which is set by the curvature of the QPC potential along the direction of current flow), the strength of electron–electron interactions  $U$ , and spin–orbit interaction  $R$ . Figure 1b depicts a conductance plateau at  $G = 2e^2/h$  for  $U = 0$  and  $R = 0$ , with an additional step developing at  $G = e^2/h$  with an in-plane magnetic field. Adding electron–electron interactions (Fig. 1c) introduces an additional feature at  $G \sim 0.7 \times 2e^2/h$ , which evolves to a plateau at  $G = e^2/h$  with magnetic field. In contrast, when SOIs are added with  $U = 0$ , the conductance at  $\mathbf{B} = 0$  is unaffected by the SOI (Fig. 1d). At finite field, the opening of a spin gap leads to a dip in conductance on the  $2e^2/h$  plateau.

Figure 1e–h shows the measured conductance of one electron and three different hole QPCs, fabricated on accumulation mode GaAs/AlGaAs heterostructures. The 1D subbands and 0.7 anomaly show the same behaviour for electrons and holes; at zero magnetic field (leftmost black trace) all QPCs exhibit clean conductance steps, quantised in integer multiples of  $2e^2/h$ . The absence of resonance structures is consistent with a low disorder, adiabatic 1D system. Applying an in-plane magnetic field parallel to the current lifts the spin degeneracy and causes additional spin split steps at  $(n + 1/2) \times 2e^2/h$ . Whereas the in-plane Zeeman splitting for electrons is isotropic<sup>4</sup>, the strong SOI in hole systems leads to a highly anisotropic Zeeman splitting for the  $n \geq 2$  subbands; the Zeeman splitting for  $\mathbf{B} \parallel \mathbf{l}$  is much bigger than that for  $\mathbf{B} \perp \mathbf{l}$ <sup>18</sup>. This anisotropy has recently been understood as a single particle effect arising from momentum-dependent mixing between light holes and heavy holes<sup>19,20</sup>. The out-of-plane  $g$ -factor is an order of magnitude larger than the in-plane  $g$ -factors, so precise alignment of the magnetic field with the 2D hole system (2DHS) is important in order to minimise orbital effects<sup>21</sup>. In this work, the magnetic field is aligned to the 2D system to better than  $0.5^\circ$ . Both electron and hole QPCs also show additional structure below the first subband, indicated by arrows in Fig. 1e–h. In all devices this feature evolves smoothly from  $0.7$  to  $0.5 \times 2e^2/h$  with applied magnetic field, a characteristic signature of the 0.7 anomaly. Further evidence that the feature observed in the hole QPCs has the same origin as the 0.7 anomaly in electron QPCs comes from the non-linear differential conductance, which shows the same zero bias peak as observed in electrons<sup>22,23</sup>. Additionally, the reduced conductance in the vicinity of the 0.7 anomaly scales as  $(1 - \mathbf{B}^2)$ , consistent with behaviour of the 0.7 anomaly identified in ref. 24 (see Supplementary Information Section 3).

In contrast to the linear response conductance, which is the same for electrons and holes, the strong SOI fundamentally alters the energy-dependent behaviour of the first 1D subband in magnetic field, as shown in Fig. 2. The transconductance  $dG/dV_g$  probes the local density of states in the QPC, and is routinely used to map the 1D subband edges as a function of energy (gate voltage). Figure 2a–f shows the transconductance colour maps, plotted against gate voltage and magnetic field for the same four QPC devices in Fig. 1e–h. In Fig. 2a, all the first three 1D electron subbands spin-split linearly in magnetic field, with no qualitative difference between the subbands. The arrow indicates the position of the 0.7 anomaly. In contrast, the 1D hole systems in Fig. 2b–d show a linear spin-splitting of the second and third subbands, while the splitting of the first subband is almost unaffected by the



**Fig. 1** 1D conductance in a QPC in magnetic field with spin-orbit and many-body interactions. **a** Schematic of a quantum point contact (QPC), with two gate electrodes biased to define a narrow one-dimensional constriction by locally depleting the 2D electron or hole system in the 2D GaAs/Al<sub>x</sub>Ga<sub>1-x</sub>As heterostructure. **b** Schematic showing how the conductance  $G$  of non-interacting electrons in a saddlepoint potential would evolve according to the Landauer-Büttiker model, with a smooth rise from 0 to  $2 \times 2e^2/h$  as the gate potential  $V_g$  (scaled by the curvature of the 1D constriction  $\Omega_x$ ) is made more negative. Application of an in-plane magnetic field  $\mathbf{B}$  creates an additional step at  $G = 0.5 \times 2e^2/h$ . **c** Schematic showing the effect of adding electron-electron interactions, which causes a characteristic shoulder-like anomaly at  $0.7 \times 2e^2/h$  to appear at  $\mathbf{B} = 0$ . This evolves to  $0.5 \times 2e^2/h$  in magnetic field, as indicated by the black arrows. **d** Including strong SOI with no electron-electron interactions does not change the situation for the non-SOI case at  $\mathbf{B} = 0$ . For  $\mathbf{B} > 0$  the conductance rises from 0 to  $2e^2/h$ , then dips as the Fermi energy moves through the spin gap in the dispersion relation. **e** Measurements of 1D electrons in a QPC, with a waterfall plot of the conductance showing the evolution of the quantisation from  $2e^2/h$  at  $\mathbf{B} = 0$  (black trace) to  $e^2/h$  in in-plane magnetic field ( $\mathbf{B}||I$ ) up to 5 T (red trace). Traces are offset horizontally for clarity. The 0.7 anomaly is indicated with the black arrow for the  $\mathbf{B} = 0$  trace, and evolves to  $0.5 \times 2e^2/h$ . **f-h** Measurements of 1D holes in three different QPCs (labelled hole QPCs 1-3) from two different wafers. Waterfall plots show evolution of the conductance quantisation from  $2e^2/h$  at  $\mathbf{B} = 0$  (black trace) to  $e^2/h$  with in-plane magnetic field up to 10 T (red trace). The field is applied  $\mathbf{B}||I$  ( $\mathbf{B} \perp \mathbf{B}_{SOI}$ ) and traces are offset in  $V_g$  for clarity. The 0.7 anomaly is indicated with the black arrow for the  $\mathbf{B} = 0$  trace, and evolves to  $0.5 \times 2e^2/h$ .



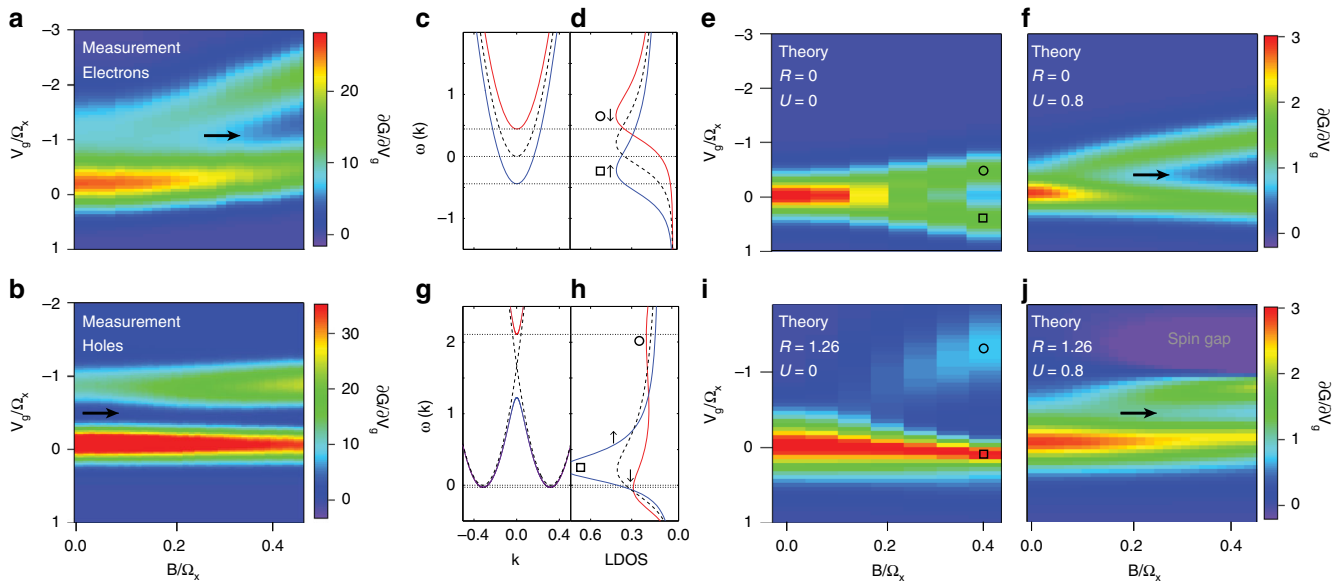
**Fig. 2** Measured transconductance  $\partial G/\partial V_g$  of the first three 1D subbands for electrons and holes in QPCs, as a function of energy (gate voltage) and magnetic field. **a** Experimental data from an electron QPC, showing a transconductance colour map of the Zeeman spin splitting of the first three 1D subbands as a function of gate voltage  $V_g$  and magnetic field  $\mathbf{B}$ . Dark-blue regions correspond to conductance plateaus, and the green to red regions correspond to conductance risers (which mark the subband edges). The dashed white boxes in **(a)** and **(b)** mark the first subband and are examined in greater detail in Fig. 3. Each subband splits linearly in magnetic field, including the 0.7 anomaly (indicated by the black arrow). **b-d** Experimental transconductance colour maps of the Zeeman spin splitting of the first three 1D hole subbands for hole QPCs 1-3. In all the cases, subbands 2 and 3 spin-split linearly in magnetic field, whereas the first hole subband is only weakly affected by the magnetic field.

magnetic field. We note that the conductance behaviour in Fig. 1f-h and transconductance behaviour in Fig. 2b-d is reproduced for a further three hole QPCs in Supplementary Information Section 4, and has also been observed in previous studies, although it has remained unexplained<sup>21,25,26</sup>.

In Fig. 3a we zoom in on the first 1D electron subband from Fig. 2a, and compare it directly to Fig. 3b where we zoom in on the first 1D hole subband of hole QPC 1 from Fig. 2b. In both Fig. 3a and b, the gate voltage and magnetic field axes have been scaled with  $\Omega_x$  to allow comparison with theory. Close up, the

differences between electrons and holes become very clear; the first 1D electron subband has a weakly resolved 0.7 anomaly structure at  $\mathbf{B} = 0$  that splits in magnetic field. In contrast, the first 1D hole subband has a strongly resolved 0.7 anomaly structure at  $\mathbf{B} = 0$  that does not broaden in energy as magnetic field increases, along with the two transconductance peaks that do not split.

The apparent suppression of the spin-splitting in the first 1D hole subband is unexpected, since the magnetic field strongly affects the conductance of the first 1D hole subband, as shown in



**Fig. 3 Comparison of measured 1D transconductance to tight-binding numerical calculations.** **a** Close up of the measured transconductance of the first 1D subband in the electron QPC (the region in the white dashed box in Fig. 2a), showing the first 1D electron subband spin-splits in magnetic field. Gate voltage  $V_g$  and magnetic field  $\mathbf{B}$  axes are converted to energy and scaled with the QPC constriction curvature parameter  $\Omega_x$  for comparison with theory. **b** Close up of the measured transconductance from hole QPC 1 (the region in the white dashed box in Fig. 2b), showing the transconductance of the first 1D hole subband is clearly different to electron QPCs, and does not split in magnetic field. **c** Calculated dispersion relation of the first spin-resolved subband (spin-up shown in blue, spin-down in red) in  $\mathbf{B} > 0$ . The vertical axis is energy  $\omega$  and the horizontal axis is wavevector  $\mathbf{k}$ . The  $\mathbf{B} = 0$  dispersion relation is indicated by the black dotted line. **d** The local density of states (LDOS) calculated from the dispersion relation shown in (c), plotted against energy  $E$ . Again the LDOS is shown for each resolved spin-species in blue and red (indicated by the up and down arrows), and the black dotted line is the LDOS in zero magnetic field. **e** Calculated transconductance colour map of the first 1D subband with no Rashba SOI ( $R = 0$ ) and no on-site Coulomb interactions ( $U = 0$ ). The circle and square markers correspond to the two spin-resolved peaks in the LDOS in (d). **f** Calculated transconductance colour map of the first 1D subband with no Rashba SOI and finite on-site Coulomb interactions  $U = 0.8$ . The 0.7 anomaly is indicated by the black arrow. **g** Calculated dispersion relation of the first subband with spin-mixing in magnetic field. The pure spin-states are indicated by the red and blue regions in the dispersion relation at  $\mathbf{k} = 0$ . The spin-mixed states are indicated by the purple regions away from  $\mathbf{k} = 0$ . **h** The LDOS for the dispersion model shown in (g). For  $\mathbf{B} > 0$ , the spin-up species in blue forms a single large peak, while the spin-down species in red forms two smaller peaks, with the peak at low energy emerging because of spin-mixing. **i** Calculated transconductance colour map of the first 1D subband with Rashba SOI  $R = 1.26$  and zero on-site Coulomb interactions  $U = 0$ . Circle and square markers correspond to the LDOS peaks indicated by the same markers in panel (h). **j** Calculated transconductance colour map of the first 1D subband with Rashba SOI magnitude  $R = 1.26$ .

Fig. 1f–h, indicating that the  $g$ -factor cannot be zero. We also cannot attribute this behaviour to peculiarities of the in-plane  $g$ -factor anisotropy; even if  $\mathbf{B}$  is applied out-of-plane, where the  $g$ -factor is an order of magnitude larger than the in-plane  $g$ -factors, the first subband shows no spin-splitting of transconductance up to 0.9 T, whereas the higher subbands have already entered the quantum Hall regime (see Supplementary Information Section 3).

To understand the difference between electron and hole systems in the 1D limit we study an infinite tight-binding chain at zero temperature in the presence of SOIs and an external magnetic field<sup>17</sup>. The first subband of the QPC is modelled as a smooth potential barrier, which is non-zero only in a finite region, separating two semi-infinite leads. Electron–electron interactions are also present only in the central QPC region of the system. Without electron–electron interactions this model is exactly solvable, while the interacting model can be studied using functional renormalisation group (fRG) theory. This model has been used for electron QPCs to reproduce the observed conductance of the 0.7 anomaly, as well as for reproducing the shot noise and compressibility, due to increased electron–electron interactions, inelastic scattering, and increased magnetic susceptibility<sup>24</sup>. This model has been extended to ‘heavy’ electrons with the inclusion of a Rashba SOI term to make predictions for the 0.7 anomaly in hole QPCs.<sup>17</sup>

Assuming (without loss of generality) that for carriers travelling in the  $x$ -direction the effective spin–orbit field  $\mathbf{B}_{\text{SOI}}$  is parallel

to the  $y$ -axis, the Rashba energy contribution equals  $-\alpha\sigma_y\mathbf{k}$ , where  $\mathbf{k}$  is the momentum of the electron,  $\alpha$  characterises the strength of the SOI, and  $\sigma_y$  is a Pauli matrix. Without an external magnetic field, this contribution results in a negative energy offset in the dispersion relation of magnitude  $\Delta E_{\text{SOI}} = \alpha^2 m^*/2\hbar^2$ , where  $m^*$  is the effective mass of the charge carriers. We parameterise the Rashba SOI by the dimensionless number  $\mathcal{R}$ ,

$$\mathcal{R} = \sqrt{\frac{\Delta E_{\text{SOI}}}{\Omega_x}} = \frac{\alpha_R}{\hbar} \sqrt{\frac{m^*}{2\Omega_x}}, \quad (1)$$

Further details of the model are given in Supplementary Information Section 1 and in refs. 17,24. We note that a strong SOI is a necessary, but not sufficient, condition to observe a spin gap in the conductance; the simple picture of the spin gap causing a conductance dip from  $2e^2/h$  to  $e^2/h$  with an applied field assumes an infinitely long, translationally invariant quantum wire. A finite-length system will, in practice, exhibit a much weaker conductance dip due to lifetime broadening of the 1D eigenstates in the wire<sup>14,17</sup>. Physical insight into the effective strength of the SOI in the 1D channel,  $\mathcal{R}$ , can be obtained by re-expressing Eq. (1) as

$$\mathcal{R} \propto \sqrt{\frac{\Delta E_{\text{SOI}}}{\hbar/\tau_{\text{transit}}}} \quad (2)$$

where  $\Delta E_{\text{SOI}}$  is the size of the spin gap, and  $\hbar/\tau_{\text{transit}}$  is the energy uncertainty arising from the finite lifetime of ballistic charge

carriers moving through the finite length 1D constriction. If this energy broadening is larger than  $\Delta E_{\text{SOI}}$ , i.e.  $\mathcal{R} < 1$ , then the spin gap cannot be resolved. Even if  $\mathcal{R} > 1$  the spin gap may only cause a small dip in the conductance.

We start our discussion with the ‘simple’ case of the first 1D electron subband, where there is no SOI, in the presence of a magnetic field  $\mathbf{B}$ . The 1D subband dispersion for non-interacting electrons is parabolic and spin-resolved in energy due to Zeeman spin-splitting, as shown in Fig. 3c. The local 1D density of states (LDOS) at the top of the barrier is shown for the two spin species in Fig. 3d. The open circle and open square indicate the spin-split peaks in the LDOS. The transconductance is a direct probe of the LDOS; the calculated transconductance colour map in Fig. 3e shows a linear splitting of the transconductance peaks with field  $\mathbf{B}$ . The absence of electron–electron interactions means there is no 0.7 anomaly. In Fig. 3f we include a finite on-site Coulomb interaction  $U = 0.8$ . This causes an enhanced and asymmetric splitting of the transconductance peaks, consistent with an enhanced spin susceptibility, and in good agreement with measurements of the 1D electron device in an in-plane magnetic field shown in Fig. 3a. The on-site Coulomb interaction also gives rise to the 0.7 anomaly at finite field.

In Fig. 3g onward, we now include a strong SOI where the Rashba SOI coefficient  $\alpha_R = 0.3$ , which is equivalent to  $\mathcal{R} = 1.26$ , consistent with the estimated strength of the SOI in the 2D hole system and the confining potential in the 1D QPC (see Supplementary Information Section 3). At zero magnetic field the 1D subbands are separated in momentum by  $\pm k_{\text{SOI}}$  due to the Rashba interaction. Applying a magnetic field parallel to the current causes spin-mixing and the opening of a spin gap at  $\mathbf{k} = 0$  in the 1D hole dispersion, as shown in Fig. 3g. This spin-mixing causes a strong enhancement of the low energy peak in the spin-‘up’ LDOS ( $\square$ ), while the spin-‘down’ LDOS splits into two smaller peaks: one below the enhanced spin-‘up’ peak, and one higher in energy ( $\circ$ ) (Fig. 3h). This splitting of the spin-‘down’ LDOS peak, with the resultant suppression in the LDOS in the vicinity of  $\omega(\mathbf{k}) = 1.2$ , corresponds to the spin gap in the dispersion relation in Fig. 3g. The higher energy peak in the LDOS ( $\circ$ ) marks the energy at which the spin gap closes.

Spin-mixing of the Rashba split bands means that the energies of the low-energy spin-‘down’ peak and the enhanced spin-‘up’ peak ( $\square$ ) are only very weakly dependent on magnetic field; they are effectively ‘pinned’ with respect to energy. This pinning is evident when we plot the transconductance in Fig. 3i, where there is a strong, single first subband peak ( $\square$ ) that hardly moves in energy. The weaker peak that is higher in energy ( $\circ$ ) in transconductance emerges in finite  $\mathbf{B}$  and then moves rapidly up in energy as  $\mathbf{B}$  increases. Again, the absence of electron–electron interactions means there is no 0.7 anomaly.

In Fig. 3j we turn on the Coulomb interactions, which significantly changes the behaviour of the transconductance. The enhanced spin-‘up’ peak and the low-energy spin-‘down’ peak that formed one large peak in Fig. 3i now form two transconductance peaks that run parallel to each other in magnetic field, with the 0.7 anomaly in between (marked by the black arrow) that does not shift in gate voltage (energy). The enhanced magnetic susceptibility strengthens the spin gap, making it visible at lower magnetic field, as indicated by the purple region in the top right of Fig. 3j. The key features of spin-orbit and electron–electron interactions in combination are the pinning of the two transconductance peaks, and the formation of a spin gap feature in the transconductance. These features are distinct from the observed transconductance in electron devices where SOI is weak or close to zero.

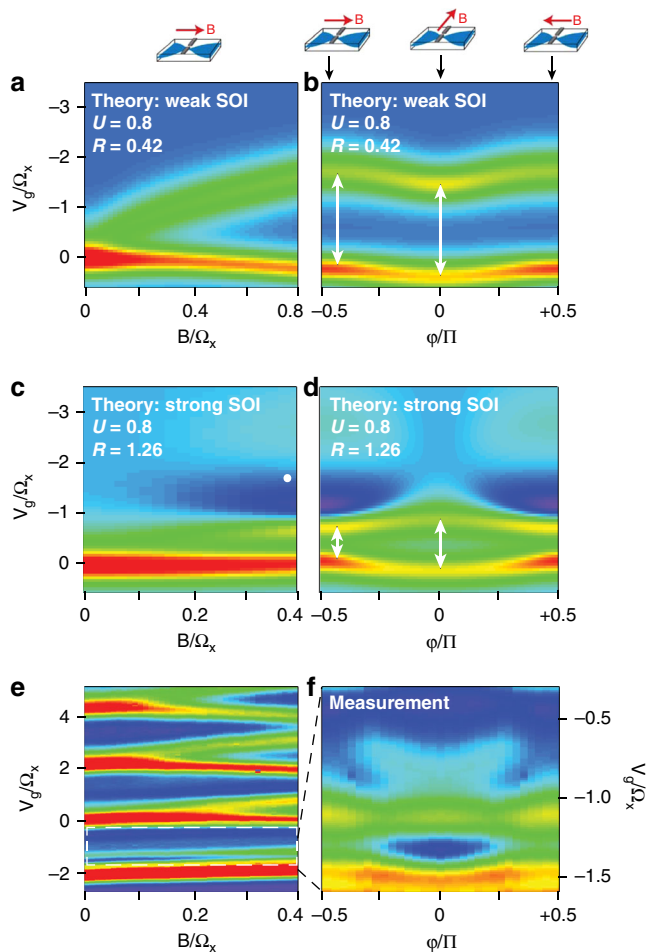
The pinning of the transconductance peaks and 0.7 anomaly produced in calculations is in very close agreement with the

observed behaviour of the first 1D hole subband transconductance in Fig. 3b, and is compelling evidence for the SOI in our hole QPCs being sufficiently strong to open a spin gap. We note that although the  $T = 0$  fRG calculations are unable to fully reproduce the  $T > 0$  experimental behaviour of the 0.7 anomaly at  $\mathbf{B} = 0$  (see refs. 17,24 and Supplementary Information Section 1), we do expect and observe good agreement at finite  $\mathbf{B}$  where both the 0.7 anomaly and spin gap are present. The absence of an observable spin-gap signature in the conductance across all six of the hole QPCs presented here and in Supplementary Information Section 4 indicates that simply applying a magnetic field along a 1D system may not be a reliable method of detecting spin gap physics. A new spin-gap signature could therefore be a valuable tool for studying spin physics in 1D systems.

If the pinning of the first two transconductance peaks is related to strong SOIs and the opening of a spin gap, it should be extremely sensitive to the orientation of the in-plane magnetic field, since the spin gap will close if  $\mathbf{B} \parallel \mathbf{B}_{\text{SOI}}$ . Figure. 4 shows the calculated and measured angular dependence of the transconductance. We start by considering  $\mathcal{R} = 0.42$  ( $\alpha_R = 0.1$ ), for which we do not expect to observe spin gap physics (due to lifetime broadening). Figure. 4a shows the first 1D subband transconductance peak splitting as the magnetic field applied parallel to the current direction is increased up to  $|\mathbf{B}| = 0.2\Omega_x$ . Figure. 4b shows the evolution of these two transconductance peaks as a function of in-plane magnetic field angle  $\varphi$ , for fixed  $|\mathbf{B}|$ . Despite the presence of the SOI, the energy gap between the two peaks remains constant as a function of magnetic field orientation, as indicated by the white arrows, although both peaks shift slightly down in energy around  $\varphi = 0$  (where  $\mathbf{B} \perp \vec{T}$ ).

Increasing the strength of the SOI to  $\mathcal{R} = 1.26$  causes the picture to change dramatically, as shown in Fig. 4c, d. The transconductance peak at  $\mathbf{B} = 0$  no longer splits with increasing  $\mathbf{B}$ ; instead the peak stays almost fixed at  $V_g = 0$  in magnetic field, with the second peak emerging at  $V_g = -0.8$  at higher fields. For  $\mathbf{B} > 0.1\Omega_x$  a weak dip in the conductance around  $V_g = -2$  due to spin gap opening causes additional transition from dark blue to light blue as  $V_g$  becomes more negative, as highlighted by the white spot on the figure. Rotating the magnetic field orientation changes both the splitting of the first two transconductance peaks and the spin gap, as shown in Fig. 4d. The two blue ‘wing-like’ structures associated with the spin gap in the range  $-1 > V_g/\Omega_x > -3.5$  disappear as  $|\varphi|/\pi \rightarrow 0$ , where  $\mathbf{B} \perp \vec{T}$  and the spin gap closes. Lower in energy, the two transconductance peaks no longer have a fixed separation: the 0.7 anomaly is ‘squashed’ by the opening spin gap away from  $|\varphi|/\pi = 0$ , indicated by the short arrow. As the field is rotated towards  $|\varphi|/\pi = 0$ , the 0.7 anomaly broadens, indicated by the longer arrow. The light blue structures at high energy, and the narrowing of the 0.7 structure away from  $|\varphi|/\pi = 0$ , provide unique signatures of the spin gap.

Figure 4e shows the first 1D subband transconductance peak splitting as the magnetic field applied parallel to the current direction is increased up to  $|\mathbf{B}| = 4$  T. The transconductance peaks from the  $n \geq 2$  subbands show a characteristic Zeeman splitting, while the ones associated with the first 1D subband are almost unaffected by  $\mathbf{B}$ . However, changing the magnetic field orientation at fixed  $|\mathbf{B}| = 4$  T (the out of plane component of the magnetic field is always less than 4 mT). has a clear effect on the first 1D subband, as shown in Fig. 4f (note that Fig. 4f is taken over the field orientation range of  $|\varphi|/\pi = 0.5$  or  $90^\circ$ , and is presented as a mirror image for easy comparison with theory. For the full data set taken over  $240^\circ$  including higher subbands and further analysis of the 1D subband spacings, see Supplementary Information Section 6.). The data show the same squashing of the 0.7 anomaly away from  $|\varphi|/\pi = 0$  as in Fig. 4d. More significantly,



**Fig. 4** Transconductance of a QPC in magnetic field with spin-orbit and many-body interactions. **a** Calculated transconductance of first 1D subband with small Rashba SOI  $\mathcal{R} = 0.42$  in increasing magnetic field up to  $\mathbf{B}/\Omega_x = 0.8$ . **b** Calculated transconductance of the first 1D subband with small  $\mathcal{R} = 0.42$  as a function of magnetic field angle  $\phi$  where the magnitude of the magnetic field is fixed at  $\mathbf{B}/\Omega_x = 0.8$ . The width of the energy gap between the two transconductance peaks is indicated by the white arrows. **c** Calculated transconductance of first 1D subband with strong  $\mathcal{R} = 1.26$  (abbreviated from Fig. 3j) in increasing magnetic field up to  $\mathbf{B}/\Omega_x = 0.4$ . The white dot indicates the region corresponding to the spin gap conductance minima in the vicinity of  $\mathbf{B}/\Omega_x = 0.4$ . **d** Calculated transconductance of the first 1D subband with small  $\mathcal{R} = 1.26$  as a function of magnetic field angle  $\phi$  where the magnitude of the magnetic field is fixed at  $\mathbf{B}/\Omega_x = 0.4$ . The width of the energy gap between the two transconductance peaks is indicated again by white arrows. **e** Measured transconductance of first 1D hole subband (abbreviated from Fig. 3b) in increasing magnetic field up to  $\mathbf{B} = 4$  T. **f** Measured transconductance of the first 1D hole subband as a function of magnetic field angle  $\phi$  where the magnitude of the magnetic field is fixed at  $\mathbf{B} = 4$  T.

there are also ‘wing-like’ structures that emerge in the range  $-1 > V_g/\Omega_x > -1.5$  as  $|\phi|$  increases. We note that in the theoretical model these ‘wing-like’ structures do not occur for  $\mathcal{R} < 1$ ; they only occur for sufficiently strong SOI that the spin gap is larger than the lifetime broadening.

The main discrepancy between theory in Fig. 4d and experiment in Fig. 4f is due to the impact of the second 1D hole subband, which is not considered in our purely 1D model. The ‘wing-like’ structures associated with the spin gap are more prominent in the calculations than in the experiments, where they do not extend all the way to the edge of the figure but vanish as

$|\phi|/\pi \rightarrow \pm 0.5$  ( $\mathbf{B} \parallel \vec{T}$ ). The absence of the spin gap structure when ( $\mathbf{B} \parallel \vec{T}$ ) is consistent with the measurement shown in Fig. 3b, where a spin gap structure is not observed despite the SOI being sufficiently strong to cause the transconductance peaks to split and run parallel to each other as magnetic field is increased. We attribute the absence of an observable spin gap structure at  $\mathbf{B} \parallel \vec{T}$  to the presence of the second, spin-split 1D subband moving down in energy. The proximity of the second 1D subband to the first 1D subband in energy is shown here to be a key factor in the ‘visibility’ of any spin-gap signature, and may in part explain the ongoing difficulty in unambiguously detecting spin-gap signatures in QPCs. This problem may be exacerbated in higher 1D subbands where the 1D subband spacing is much smaller than the first and second 1D subband spacing, and spin-gap signatures have been predicted to occur but have not been observed<sup>27</sup>. Further analysis and discussion of the higher 1D hole subbands is provided in Supplementary Information Section 6.

## Discussion

In experimental systems strong electron–electron interactions are always present in the 1D limit, and so must be considered on an equal footing with the SOI. Our measurements of the first 1D subband in QPCs with and without strong SOI demonstrate that the SOI fundamentally alters the behaviour of the first 1D hole subband compared to the first 1D electron subband. The experimental data and the modelling both show that the magnetic field evolution of the transconductance is a much more sensitive probe of the spin gap than the conductance. Although the model does not contain some of the more complex spin-physics of holes, it nevertheless reproduces the key experimental observations: (i) despite the magnetic field causing the 0.7 anomaly to evolve towards  $0.5 \times 2e^2/h$ , the associated transconductance peaks remain pinned in energy and hardly change as  $\mathbf{B}$  is increased, and (ii) rotating the magnetic field causes characteristic features to appear in the transconductance.

By comparing the experimental data of Figs. 2–4 with theory we can obtain an estimate of the spin–orbit gap. We calculated the transconductance for a range of SOI values  $0 \leq \mathcal{R} \leq 1.26$ , electron–electron interaction strengths  $0 \leq U \leq 0.8$ , and magnetic fields  $0 \leq \mathbf{B} \leq 0.88\Omega_x$  and then compared them to the measured transconductance. We found  $\mathcal{R} = 1.26$  and  $U = 0.8$  to be in closest agreement with experiment in Fig. 3j and  $\mathbf{B} = 0.4\Omega_x$  in Fig. 4d. Using  $\mathcal{R} = 1.26$  and Eq. (1), we estimate the size of the spin gap in the device in Fig. 3b to be  $\Delta E = 550 \pm 100 \mu\text{eV}$ . This is consistent with the value expected from independent measurements of the Rashba splitting in the 2D hole system (see Supplementary Information Section 3).

Finally, we remark on the impact of this work on topological superconductivity and Majorana physics in 1D systems. To enter the topological regime strong SOI, low disorder and superconducting contacts are prerequisites. The wing-like structure shown in Fig. 4 is a universal and unambiguous signature of the spin gap, and can be used to tune the system into the topological regime. Our work also shows that the effective strength of the SOI in the 1D system should be large (the 1D system should be as long as possible while maintaining ballistic transport, to maximise  $\mathcal{R}$ ), and the 1D subband spacing should be maximised. With the recent demonstration of superconducting contacts to ultra-low disorder 2D electron systems in GaAs/AlGaAs heterostructures, and to high mobility holes in Ge quantum wells<sup>28,29</sup>, this work shows a route to scalable topological superconducting circuits.

## Methods

**Experimental set-up.** All devices for these experiments were fabricated on undoped accumulation mode (100) GaAs/Al<sub>x</sub>Ga<sub>1-x</sub>As heterostructures, using

standard electron beam lithography techniques to define the QPCs. Details of all the wafers used and dimensions of the QPCs, are given in Supplementary Information Section 4. Measurements were performed in dilution refrigerators with base temperatures below 40 mK, using standard low-frequency ac lock-in techniques with an applied excitation voltage of  $V_{sd} = 50$  to  $100 \mu\text{V}$ , where typically more than half of  $V_{sd}$  is dissipated across the 2DEG/2DHG, ohmic contacts and cold filters. Typical electron and hole densities were from  $1.0$  to  $2.5 \times 10^{11} \text{ cm}^{-2}$ , with electron and hole mobilities above  $1 \times 10^6 \text{ cm}^2 \text{ V}^{-1} \text{ s}^{-1}$ .

### Data availability

The data that support the findings of this study are available from the corresponding author upon reasonable request.

Received: 14 July 2020; Accepted: 12 October 2020;

Published online: 04 January 2021

### References

- Wharam, D. A. et al. One-dimensional transport and the quantisation of the ballistic resistance. *J. Phys. C* **21**, L209 (1988).
- van Wees, B. J. et al. Quantized conductance of point contacts in a two-dimensional electron gas. *Phys. Rev. Lett.* **60**, 848–850 (1988).
- Büttiker, M. Four-terminal phase-coherent conductance. *Phys. Rev. Lett.* **57**, 1761–1764 (1986).
- Thomas, K. J. et al. Possible spin polarization in a one-dimensional electron gas. *Phys. Rev. Lett.* **77**, 135–138 (1996).
- Micolich, A. P. What lurks below the last plateau: experimental studies of the  $0.7 \times 2e^2/h$  conductance anomaly in one-dimensional systems. *J. Phys.: Condens. Matter* **23**, 443201 (2011).
- Auslaender, O. M. et al. Spin-charge separation and localization in one dimension. *Science* **308**, 88–92 (2005).
- Jompol, Y. et al. Probing spin-charge separation in a Tomonaga-Luttinger liquid. *Science* **325**, 597–601 (2009).
- Kitaev, A. Y. Unpaired majorana fermions in quantum wires. *Phys.-Uspekhi* **44**, 131–136 (2001).
- Sau, J. D., Lutchyn, R. M., Tewari, S. & Sarma, S. D. Generic new platform for topological quantum computation using semiconductor heterostructures. *Phys. Rev. Lett.* **104**, 040502 (2010).
- Oreg, Y., Refael, G. & vonOppen, F. Helical liquids and majorana bound states in quantum wires. *Phys. Rev. Lett.* **105**, 177002 (2010).
- Quay, C. H. L. et al. Observation of a one-dimensional spin-orbit gap in a quantum wire. *Nat. Phys.* **6**, 336 EP - (2010).
- Heedt, S. et al. Signatures of interaction-induced helical gaps in nanowire quantum point contacts. *Nat. Phys.* **13**, 563–567 (2017).
- Kammhuber, J. et al. Conductance through a helical state in an Indium antimonide nanowire. *Nat. Commun.* **8**, 478 (2017).
- Rainis, D. & Loss, D. Conductance behavior in nanowires with spin-orbit interaction: a numerical study. *Phys. Rev. B* **90**, 235415 (2014).
- Heyder, J. et al. Relation between the 0.7 anomaly and the Kondo effect: geometric crossover between a quantum point contact and a Kondo quantum dot. *Phys. Rev. B* **92**, 195401 (2015).
- Winkler, R. *Spin-orbit Coupling Effects in Two-dimensional Electron and Hole Systems*. Springer Tracts in Modern Physics (Springer, Berlin, 2003).
- Goulko, O., Bauer, F., Heyder, J. & vonDelft, J. Effect of spin-orbit interactions on the 0.7 anomaly in quantum point contacts. *Phys. Rev. Lett.* **113**, 266402 (2014).
- Danneau, R. et al. Zeeman splitting in ballistic hole quantum wires. *Phys. Rev. Lett.* **97**, 026403 (2006).
- Miserev, D. S. et al. Mechanisms for strong anisotropy of in-plane  $g$ -factors in hole based quantum point contacts. *Phys. Rev. Lett.* **119**, 116803 (2017).
- Srinivasan, A. et al. Detection and control of spin-orbit interactions in a GaAs hole quantum point contact. *Phys. Rev. Lett.* **118**, 146801 (2017).
- Nichele, F. et al. Characterization of spin-orbit interactions of GaAs heavy holes using a quantum point contact. *Phys. Rev. Lett.* **113**, 046801 (2014).
- Cronenwett, S. M., Oosterkamp, T. H. & Kouwenhoven, L. P. A tunable Kondo effect in quantum dots. *Science* **281**, 540–544 (1998).
- Wieck, A. D., Batke, E., Heitmann, D., Kotthaus, J. P. & Bangert, E. Lifting of the spin degeneracy of hole subbands in a surface electric field on silicon. *Phys. Rev. Lett.* **53**, 493–496 (1984).
- Bauer, F. et al. Microscopic origin of the ‘0.7-anomaly’ in quantum point contacts. *Nature* **501**, 73–78 (2013).
- Chen, J. C. H. et al. Observation of orientation- and k-dependent Zeeman spin-splitting in hole quantum wires on (100)-oriented AlGaAs/GaAs heterostructures. *N. J. Phys.* **12**, 033043 (2010).
- Komijani, Y. et al. Anisotropic Zeeman shift in p-type GaAs quantum point contacts. *EPL (Europhys. Lett.)* **102**, 37002 (2013).
- Pershin, Y. V., Nesteroff, J. A. & Privman, V. Effect of spin-orbit interaction and in-plane magnetic field on the conductance of a quasi-one-dimensional system. *Phys. Rev. B* **69**, 121306-1–121306-4 (2004).
- Wan, Z. et al. Induced superconductivity in high-mobility two-dimensional electron gas in gallium arsenide heterostructures. *Nat. Commun.* **6**, 7426 EP (2015).
- Hendrickx, N. W. et al. Gate-controlled quantum dots and superconductivity in planar germanium. *Nat. Commun.* **9**, 2835 (2018).

### Acknowledgements

We gratefully acknowledge T. Li, V. Richards and A. Laucht for helpful discussions. This work was funded by the Australian Research Council (ARC) through the Discovery Projects Scheme and the ARC Centre of Excellence in Future Low-Energy Electronics Technologies (CE170100039). J. von Delft acknowledges support from the Deutsche Forschungsgemeinschaft under Germany’s Excellence Strategy, EXC-2111–390814868. D. A. Ritchie acknowledges support from the Engineering and Physical Sciences Research Council, United Kingdom.

### Author contributions

Q.W., A.S. and L.A.Y. fabricated the samples. K.L.H. and A.S. performed the measurements. O.G. derived the theoretical model with input from J.v-D.I.F., D.A.R., A.L. and A.D.W. supplied the heterostructure wafers. K.L.H. analysed the data with input from A.R.H., A.S. and O.K. K.L.H. and A.R.H. wrote the manuscript with input from all authors.

### Competing interests

The authors declare no competing interests.

### Additional information

Supplementary information is available for this paper at <https://doi.org/10.1038/s41467-020-19895-3>.

Correspondence and requests for materials should be addressed to A.R.H.

Peer review information *Nature Communications* thanks the anonymous reviewer(s) for their contribution to the peer review of this work.

Reprints and permission information is available at <http://www.nature.com/reprints>

Publisher’s note Springer Nature remains neutral with regard to jurisdictional claims in published maps and institutional affiliations.



**Open Access** This article is licensed under a Creative Commons Attribution 4.0 International License, which permits use, sharing, adaptation, distribution and reproduction in any medium or format, as long as you give appropriate credit to the original author(s) and the source, provide a link to the Creative Commons license, and indicate if changes were made. The images or other third party material in this article are included in the article’s Creative Commons license, unless indicated otherwise in a credit line to the material. If material is not included in the article’s Creative Commons license and your intended use is not permitted by statutory regulation or exceeds the permitted use, you will need to obtain permission directly from the copyright holder. To view a copy of this license, visit <http://creativecommons.org/licenses/by/4.0/>.

© The Author(s) 2021

# Supplementary Information: New signatures of the spin gap in quantum point contacts

K. L. Hudson<sup>1,2</sup>, A. Srinivasan<sup>1,2</sup>, O. Goulko<sup>3</sup>, J. Adam<sup>1</sup>, Q. Wang<sup>1,2</sup>, L. A. Yeoh<sup>1</sup>, O. Klochan<sup>1,2</sup>,  
I. Farrer<sup>4</sup>, D. A. Ritchie<sup>5</sup>, A. Ludwig<sup>6</sup>, A.D. Wieck<sup>6</sup>, J. von Delft<sup>7</sup> & A. R. Hamilton<sup>1,2\*</sup>

<sup>1</sup>*School of Physics, University of New South Wales, Sydney, NSW, 2052, Australia.*

<sup>2</sup>*ARC Centre of Excellence in Future Low-Energy Electronics Technologies, University of New South Wales, Sydney, NSW, 2052, Australia.*

<sup>3</sup>*Department of Physics, University of Massachusetts, Boston, MA, 02125, USA.*

<sup>4</sup>*Cavendish Laboratory, University of Cambridge, Madingley Road, Cambridge, United Kingdom.*

<sup>5</sup>*Department of Electronic and Electrical Engineering, University of Sheffield, Sheffield, United Kingdom.*

<sup>6</sup>*Angewandte Festkörperphysik, Ruhr-Universität Bochum, D-44780 Bochum, Germany*

<sup>7</sup>*Arnold Sommerfeld center for Theoretical Physics, Ludwig-Maximilians Universität, München, Theresienstrasse 37, D-80333, München, Germany.*

\*e-mail: alex.hamilton@unsw.edu.au



<b>1</b>	<b>Notes on theory</b>	<b>S-3</b>
<b>2</b>	<b>Subband properties and calculation of <math>\mathcal{R}</math> for QPCs</b>	<b>S-6</b>
<b>3</b>	<b>Further evidence of dependence of first subband with spin-orbit interaction in magnetic field</b>	<b>S-11</b>
<b>4</b>	<b>Fabrication and measurement methods</b>	<b>S-23</b>

## 1 Notes on theory

Our theoretical description <sup>1</sup> is based on the following infinite tight-binding chain Hamiltonian,

$$\begin{aligned}
H = & \sum_{j,\sigma,\sigma'} d_{j\sigma}^\dagger \left[ (V_j + 2\tau)\delta_{\sigma\sigma'} - \frac{1}{2}(\boldsymbol{\sigma} \cdot \mathbf{B})_{\sigma\sigma'} \right] d_{j\sigma'} \\
& + \sum_{j,\sigma,\sigma'} \left[ d_{j+1\sigma}^\dagger \left( -\tau_0\delta_{\sigma\sigma'} + \frac{i\alpha}{2}(\sigma_y)_{\sigma\sigma'} \right) d_{j\sigma'} + \text{h.c.} \right] \\
& + \sum_j U_j d_{j\uparrow}^\dagger d_{j\uparrow} d_{j\downarrow}^\dagger d_{j\downarrow},
\end{aligned} \tag{1}$$

where  $d_{j\sigma}$  and  $d_{j\sigma}^\dagger$  annihilate and create an electron with spin  $\sigma \in \{\uparrow, \downarrow\}$  at site  $j$ , respectively, and  $\boldsymbol{\sigma} = (\sigma_x, \sigma_y, \sigma_z)$  is a vector of Pauli matrices. The external magnetic field  $\mathbf{B}$  and spin orbit parameter  $\alpha$  are constant throughout the chain. The effective mass of the charge carrier is  $m = \hbar^2/2\tau a^2$  with  $\tau = \sqrt{\tau_0^2 + \alpha^2}$ , where  $\tau_0$  is the hopping between sites in the discrete model and  $a$  is the spacing between sites. We keep  $\tau$  fixed when varying  $\alpha$ , in order to ensure that the effective mass in the discrete model matches the physical effective mass. This is equivalent to matching the bandwidth.

In our calculations the QPC region consists of 101 sites centered around  $j = 0$  and thus has overall length  $L = 2Na$  with  $N = 50$ . Sites  $j < -N$  and  $j > N$  represent two leads with bandwidth  $4\tau$ . The QPC barrier potential,

$$V_j = V(ja) = (V_g + \mu) \exp \left[ -\frac{(2ja/L)^2}{1 - (2ja/L)^2} \right], \tag{2}$$

and the (on-site) electron-electron interaction,

$$U_j = U(ja) = U \exp \left[ -\frac{(2ja/L)^6}{1 - (2ja/L)^2} \right], \tag{3}$$

are nonzero only in the QPC region. Both the barrier potential and interaction are symmetric around the center and vanish smoothly at the boundary of the QPC region. The barrier potential is quadratic around the central site  $j = 0$ , representing the lowest QPC subband. The barrier height  $V_g$ , measured w.r.t. the chemical potential  $\mu = 2\tau$ , mimics the role of the gate-voltage. If  $V_g$  is swept downwards through zero, the linear conductance  $g$  increases from 0 to 1.

In the main paper we discuss results for the following physical quantities at zero temperature: the local density of states (LDOS),  $\mathcal{A}_{j=0}^\sigma$ , at the central site of the system (with  $U = 0$ ) and the linear conductance,  $g$ . The former is given by

$$\mathcal{A}_j^\sigma(\omega) = -\text{Im}\mathcal{G}_{jj}^{\sigma\sigma}(\omega)/\pi a, \quad (4)$$

where  $\mathcal{G}_{jj'}^{\sigma\sigma'}$  is the retarded propagator from site  $j'$  with spin  $\sigma'$  to site  $j$  with spin  $\sigma$ . Due to SOI,  $\mathcal{G}_{jj}^{\sigma\sigma'}$  is not spin-diagonal, but at  $j = 0$  its off-diagonal elements are negligible compared to the diagonal ones. The linear conductance can be calculated via <sup>2</sup>

$$g = g_1 + g_2 \propto \text{Tr}(t^\dagger t) = \sum \text{eig}(t^\dagger t), \quad (5)$$

where  $t^{\sigma\sigma'} = \mathcal{G}_{-N,N}^{\sigma\sigma'}(\mu)$  is the transmission matrix of the QPC. The eigenvalues of  $t^\dagger t$ , which yield the conductance, are independent of  $N$ .

The non-interacting system ( $U = 0$ ) can be solved exactly. In the presence of electron-electron interactions, we calculate the conductance at zero temperature with the functional Renormalization Group technique in the one-particle irreducible version <sup>3-7</sup> using the coupled ladder approximation, which was presented in Ref [8] for a model without SOI.

### **Note on $T = 0$ calculations and finite $T$ experiments**

The  $T = 0$  fRG theory captures the behaviour of the 0.7 anomaly at finite magnetic field, in good agreement with experimental data. This is the regime in which the key physics of spin gap is observed, and is the regime we concentrate on in this work. The agreement between the calculations and measurement is less good at low  $B$ , where finite  $T$  effects become more significant. Here the  $T = 0$  theory appears to show a suppression of the 0.7 anomaly at low  $B$ , which does not occur in experiment. This suppression is a limitation of the fRG technique used to solve the 1D model; finite  $T$  calculations using second order perturbation theory do not show a suppression of the 0.7 anomaly at  $T > 0, B = 0$ , but do not fully capture the electron-electron interactions, as discussed in Ref. [9].

## 2 Subband properties and calculation of $\mathcal{R}$ for QPCs

### Summary of QPC parameters

Here we summarise the gate dimensions, charge density, spin polarisation and provide and estimate of the magnitude of  $\mathcal{R}$  for each QPC device in Supplementary Tables 1 and 2. The method for calculating these values including is provided below, along with discussion about the challenges of obtaining an accurate value of  $\mathcal{R}$ .

Device	Wafer no.	2DEG/2DHG depth (nm)	$l \times w$ (nm)	$n_{2D}$ ( $10^{11}\text{cm}^{-2}$ )	$\Delta p/p$	$\mathcal{R}$	$\Delta E_{SOI}$ ( $\mu\text{eV}$ )
Electron QPC	1 [W639]	160	$60 \times 350$	1.5	0	0	0
Hole QPC 1	2 [W713]	85	$300 \times 300$	1.2	0.10	$0.7^{+0.41}_{-0.34}$	580
Hole QPC 2	3 [W917]	60	$100 \times 300$	2.5	0.46	$1.6^{+0.36}_{-0.19}$	450
Hole QPC 3	3 [W917]	60	$100 \times 300$	2.5	0.46	$1.6^{+0.36}_{-0.19}$	480
Hole QPC 4	1 [W639]	160	$200 \times 800$	2.5	0.29	$1.8^{+0.30}_{-0.35}$	250
Hole QPC 5	4 [B13180] <sup>†</sup>	200	$400 \times 400$	1.5			
Hole QPC 6	5 [W918]	60	$350 \times 350$	2.1	0.40	$2.5^{+0.18}_{-0.03}$	960

Supplementary Table 1. Summary of measured spin populations and spin-orbit parameter  $\mathcal{R}$  calculated from  $\Delta p/p$  and  $l$  for each device. <sup>†</sup> Characterisation of Rashba SOI via Shubnikov-de Haas oscillations were not performed for this wafer. No value for  $\Delta p/p$  or  $\mathcal{R}$  available.

Device	Wafer no.	2DEG/2DHG depth (nm)	$l \times w(\text{nm})$	$\Omega_y(\mu\text{eV})$	$\Omega_x(\mu\text{eV})$
Electron QPC	1 [W639]	160	$60 \times 350$	1900	600
Hole QPC 1	2 [W713]	85	$300 \times 300$	490	150
Hole QPC 2	3 [W917]	85	$100 \times 300$	475	180
Hole QPC 3	3 [W917]	85	$100 \times 300$	500	190
Hole QPC 4	1 [W639]	160	$200 \times 800$	290	75
Hole QPC 5	4 [B13180]	200	$400 \times 400$	240	110
Hole QPC 6	5 [W918]	60	$350 \times 350$	520	150

Supplementary Table 2. Summary of subband spacings  $\Omega_y$  and  $\Omega_x$  for each device.

### Calculating $\mathcal{R}$ via $\Delta p/p$ and QPC length $l$

The value of  $\mathcal{R}$  can be obtained from the measured strength of the spin-orbit interaction in the 2DEG/2DHG system and the length of the QPC. The Rashba interaction in 2D systems derived from the Luttinger Hamiltonian is:

$$H = \frac{1}{2m_e} \left( \left( \gamma_1 + \frac{5}{2}\gamma_2 \right) p^2 - 2\gamma_2 (p \cdot S)^2 \right) \quad (6)$$

The 2D potential is applied to restrict motion in the  $z$ -direction. At experimental densities, we have  $\langle p_z^2 \rangle \gg p_F^2 = p_x^2 + p_y^2$ , so that the dominant terms in (1) are proportional to  $p_z^2 S_z^2$  and are diagonal in a basis of states with definite  $S_z$ . States with  $S_z = \pm \frac{3}{2}$  (heavy holes) are split in energy from

states with  $S_z = \pm\frac{1}{2}$  (light holes). The light holes are higher in energy by a splitting equal to

$$\Delta_{HH-LH} = -\frac{2\gamma_2\langle p_z^2 \rangle}{m_e} \approx 10 \text{ meV}, \quad (7)$$

so that the low energy sector consists of a doublet of heavy holes.

The remaining terms containing  $S_x, S_y$  introduce mixing between heavy and light hole states.

Accounting for a correction in third order perturbation theory due to the terms

$$-\frac{\gamma}{m_e}((p_x S_x + p_y S_y)^2 + \{p_x S_x + p_y S_y p_z S_z\}) \quad (8)$$

we find that the interaction is of the form

$$H_R = \frac{ia}{2}(p_+^3 \sigma_- - p_-^3 \sigma_+) \quad (9)$$

where  $a$  is a numerical coefficient depending on the shape of the well. Due to parity selection rules,  $a = 0$  for a symmetric well.

The Rashba interaction splits the 2D bands. The dispersion has the form

$$\varepsilon_p^\pm = \frac{p^2}{2m} \pm \alpha p^3. \quad (10)$$

Magnetotransport experiments in 2D hole systems show two Fermi surfaces with carrier densities  $p_+$  and  $p_-$  that are typically different by a factor of two, although this factor may be as large as twenty. The strength of the Rashba interaction may be extracted in a straightforward manner.

Introducing the parameter

$$p = \sqrt{2mE_F} \quad (11)$$

we can characterise the spin-orbit interaction in terms of the dimensionless constant

$$\frac{\alpha p^3}{E_F} = 2m\alpha p \approx \frac{\alpha p_+^3}{E_F} \approx \frac{\alpha p_-^3}{E_F} \quad (12)$$

This can be solved given knowledge of  $p_+$ ,  $p_-$

$$E_F = \frac{p_+^2}{2m} - \alpha p_+^3 = \frac{p_-^2}{2m} + \alpha p_-^3 \rightarrow 2m\alpha p = p \frac{p_+^2 - p_-^2}{p_-^3 + p_+^3} \quad (13)$$

For QPC 4 (a typical experimental situation), the densities  $p_-$  and  $p_+$  are in the ratio 0.29 : 0.71.

Writing

$$p_+^2 = 0.71(2p^2), \quad p_-^2 = 0.29(2p^2) \quad (14)$$

we can substitute into (8) and find

$$2m\alpha p = \frac{(2p^2) \cdot p(0.71 - 0.29)}{(2p^2)^{\frac{3}{2}}(0.71^{\frac{3}{2}} + 0.29^{\frac{3}{2}})} = 0.28 \quad (15)$$

The large value of this dimensionless size of the spin-orbit interaction reflects the fact that, in inversion asymmetric 2D hole systems, the Rashba interaction is a considerable proportion of the kinetic energy.

In a QPC, an additional harmonic potential is applied to the confine the electrons to a 1D channel. Therefore momentum along the  $y$ -direction is quantized. We can make the substitution  $\langle p_y^2 \rangle \rightarrow 2mE_F$ ,  $\langle p_y \rangle = 0$ . Then expanding the 2D Hamiltonian we obtain

$$H_R \rightarrow -3ap_y^2 p_x \sigma_y + ap_x^3 \sigma_y \quad (16)$$

Near the top of the barrier,  $p_x \rightarrow 0$  and the first term dominates. We may write it in the form

$$H_R \rightarrow -\alpha p_x \sigma_y, \quad a = 3\alpha p_y^2 = 6m\alpha E_F \quad (17)$$



The dimensionless parameter  $\mathcal{R}$  is defined to be the ratio of  $\alpha$  to the velocity scale determined by the shape of the parabolic barrier inside the channel,  $U(x) \approx U_0 - \frac{m\Omega_x^2 x^2}{2}$

$$\mathcal{R} = \frac{\alpha}{v} = \alpha \sqrt{\frac{m}{\Omega_x}} \quad (18)$$

From the expression for the Fermi energy  $E_F$  inside the parabolic potential

$$E_F = \frac{m\Omega_x^2 l^2}{8} \rightarrow \Omega_x = \sqrt{\frac{8E_F}{ml^2}} \quad (19)$$

we can express  $\mathcal{R}$  in terms of the 1D channel length

$$\mathcal{R}^2 = \frac{m\alpha^2}{\Omega_x} = \frac{m\alpha^2}{2} \sqrt{\frac{ml^2}{2E_F}} = \frac{(m\alpha)^2}{2} \sqrt{\frac{l^2}{2mE_F}} = \frac{lp}{2} \left( \frac{m\alpha}{p} \right)^2 \quad (20)$$

Using a density of  $2.5 \times 10^{11} \text{cm}^{-2}$  and length  $l = 300 \text{nm}$  as typical values, and the value of  $2m\alpha p$  found in equation (10), we find

$$\frac{m\alpha}{p} = 3map = \frac{3}{2}(2m\alpha p) = 0.42 \quad (21)$$

This yields a final value of  $\mathcal{R}^2 = 3.3 \rightarrow \mathcal{R} \approx 1.8$ .

The main limitation of using equation (20) to estimate  $\mathcal{R}$  is the uncertainty in the true QPC length felt by the first harmonic, which will likely be longer than the lithographic gate length. The QPC length felt by the first 1D subband is determined by the electrostatic profile of the surface gates when the QPC is being squeezed, which is determined by the dimensions of the surface gates and the depth of the 2DHG. The method above provides a reasonable estimation of  $\mathcal{R}$ . However we argue that the form of the first 1D subband in magnetic field (i.e., the absence of Zeeman spin-splitting) is the most reliable indicator of  $\mathcal{R} > 1$ .

### 3 Further evidence of dependence of first subband with spin-orbit interaction in magnetic field

In this section we include Zeeman spin-splitting measurements on additional QPCs, source-drain bias, and additional analysis in the small energy limit  $\tilde{B}$  and higher subbands.

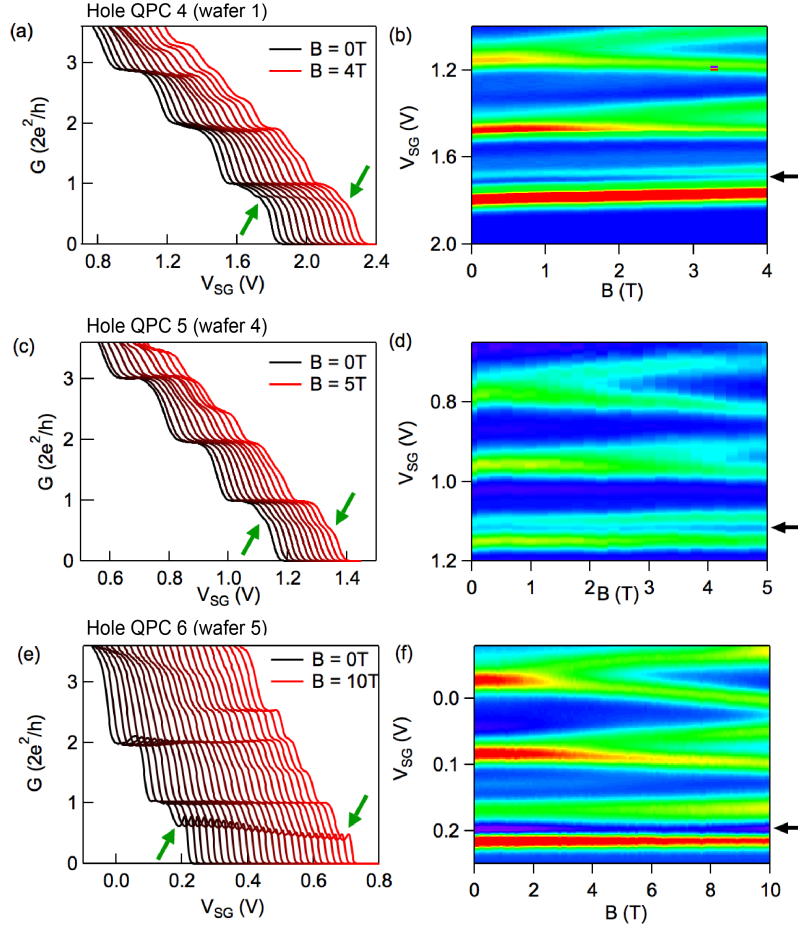
#### Additional Zeeman spin-splitting measurements

Additional Zeeman spin-splitting measurements on hole QPCs have been presented here to provide further evidence for the first 1D hole subband behaviour in magnetic field described in the main text.

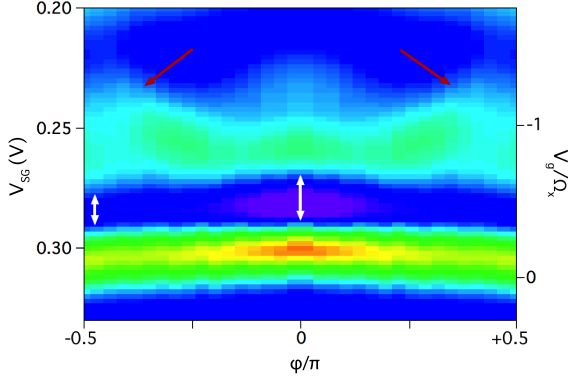
**Supplementary Figure 1** shows the conductance waterfall plots and transconductance colour maps for hole QPCs 4-6 evolving in magnetic field. The data is shown for subbands  $n = 1..3$ . Subbands  $n = 2, 3$  spin split in magnetic field, while subband  $n = 1$  has a 0.7 anomaly that evolves to  $0.5 \times 2e^2/h$  in magnetic field in field  $B > 5$  T [indicated by the green arrows in **panels (a,c,e)**]. In transconductance, subbands  $n \geq 2$  Zeeman spin-split, while the first subband remains unaffected by the magnetic field [**panels(b, d, f)**]. The 0.7 anomaly is indicated by the black arrows on the right side of **panels(b, d, f)**.

**Supplementary Figure 2** shows the angular response of the first subband in 8 T of magnetic field in hole QPC 2. Similarly to **Fig. 4f**, the data has been trimmed and reflected around  $\varphi/\pi = 0$  for easy comparison with theory. The 0.7 anomaly is broadest around  $\varphi/\pi = 0$ , and narrows at

$\varphi/\pi = \pm 0.5$  (indicated by the white arrows). The spin gap structures in the top corners of the figure (indicated by the red arrows) are greatly suppressed in QPC 1 due to the small 1D subband spacing and spin-split subband  $n = 2$ .



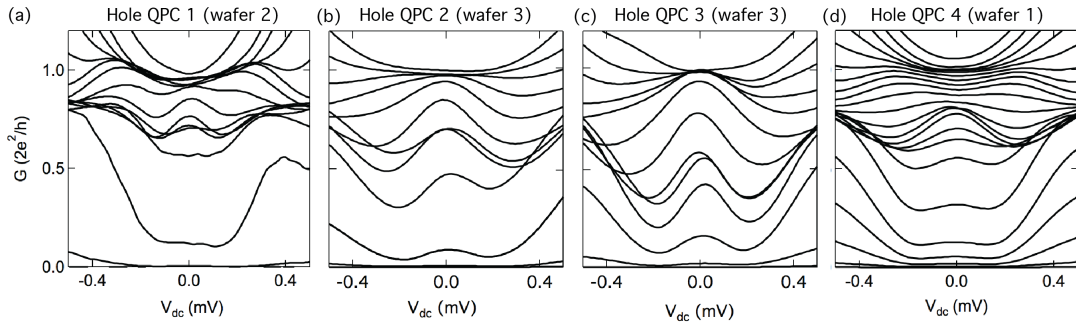
Supplementary Figure 1: (a, c, e) Waterfall plots of the conductance of 1D holes in hole QPCs 4-6 respectively, showing the evolution of the quantization from  $2e^2/h$  at  $B = 0T$  (black trace) to  $e^2/h$  in in-plane  $B \perp B_{SOI}$  magnetic field up to 10T (red trace). Traces are offset in  $V_{SG}$  for clarity. The 0.7 anomaly is indicated with the black arrow for the  $B = 0T$  trace, and evolves in  $0.5 \times G$ . (b, d, f) Experimental transconductance colour maps of the Zeeman spin splitting of the first three 1D hole subbands for three different QPC devices. In all cases subbands 2 and 3 spin-split linearly in magnetic field, whereas the first hole subband is only weakly affected by the magnetic field.



Supplementary Figure 2: Measured transconductance of the first 1D hole subband in hole QPC 2 as a function of magnetic field angle  $\varphi$  where the magnitude of the magnetic field is fixed at  $B = 8$  T. Vertical axis is gate voltage scaled by  $\Omega_x$ , and horizontal axis is magnetic field angle with respect to  $B_{SOI}$ . The white arrows indicate the breadth of the 0.7 anomaly. The red arrows indicate the transconductance structures corresponding to the spin gap emerging in the top corners of the figure.

## The Zero-Bias Anomaly

The zero-bias anomaly (ZBA) is intimately linked to the 0.7 anomaly<sup>9,10</sup>. To confirm that the feature observed in the hole QPCs has the same origin as the 0.7 anomaly in electron QPCs we show the non-linear differential conductance as a function of source-drain bias for hole QPCs in **Supplementary Figure 3**. At low conductances  $G < 0.7 \times 2e^2/h$ , there is a peak centred around zero bias, consistent with the 0.7 anomaly and zero bias peak reported in electron QPCs<sup>10</sup>.



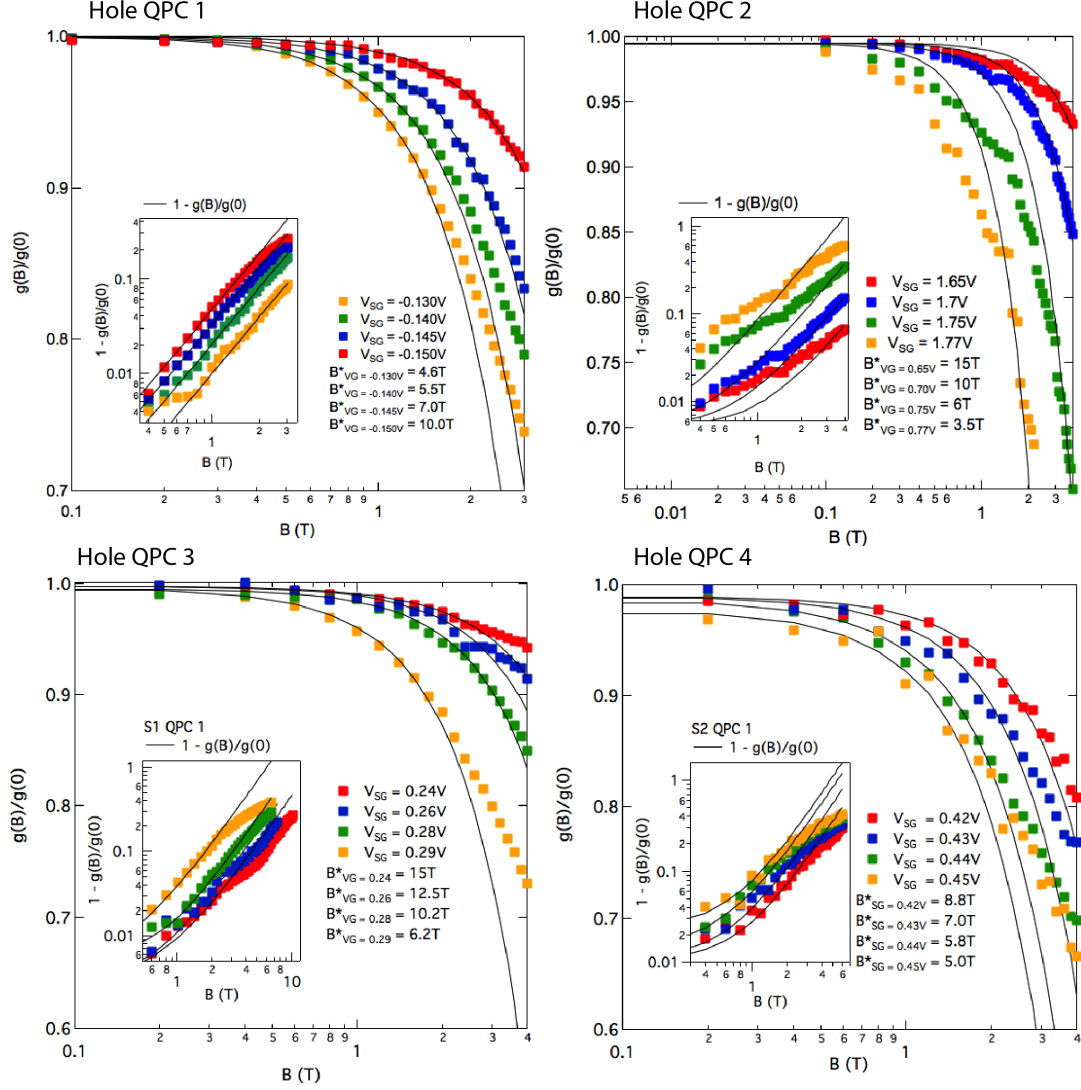
Supplementary Figure 3: Non-linear differential conductance  $G$  as a function of dc voltage  $V_{dc}$  for a range of side-gate bias values (or QPC width) for hole QPCs 1-4. In each QPC device there is a conductance peak centered around  $V_{dc} = 0$  that splits into two peaks where  $0.7 \times (2e^2/h) > G > (2e^2/h)$ .

### Limit of small energy $\tilde{B}$

Modelling of the first 1D electron subband in Ref [9] using (SOPT) yields the following prediction: that for fixed values of side gate voltage  $V_{sg}$ , or 1D confinement, the leading dependence of the non-linear conductance on  $\tilde{B}$  is quadratic. The quadratic relation takes the form

$$\frac{g_{nl}(\tilde{B}, \tilde{T}, \tilde{V}_{sd})}{g_{nl}(0, 0, 0)} \approx 1 - \frac{\tilde{B}^2}{\tilde{B}_*^2} - \frac{\tilde{T}^2}{\tilde{T}_*^2} - \frac{\tilde{V}_{sd}^2}{\tilde{V}_{sd*}^2} \quad (22)$$

where  $\tilde{B}/\tilde{B}_* \ll 1$  and  $\tilde{B}_*$ ,  $\tilde{T}_*$  and  $\tilde{V}_{sd*}$  are  $V_{sg}$  dependent crossover scales that govern the strength of the 0.7 anomaly for finite exchange interaction energies. We demonstrate here that the relationship holds for the hole 0.7 anomaly with SOI in **Supplementary Figure 4**.



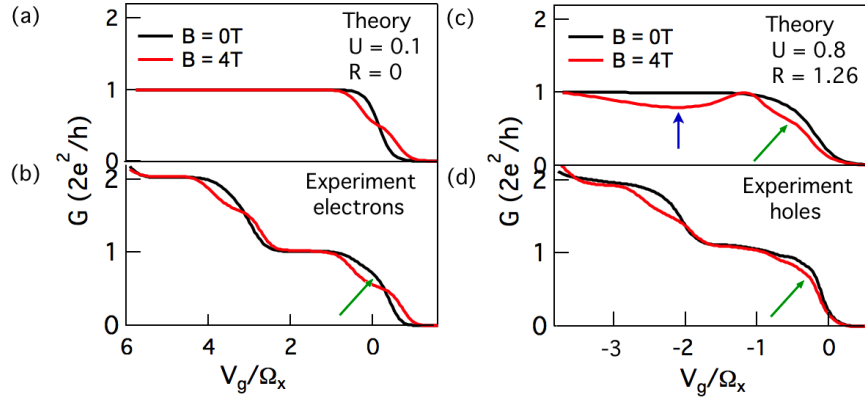
Supplementary Figure 4:  $g(B)/g(0)$  as a function of  $B$  for a range of top gate voltages (densities) for hole QPCs 1-4 in (a-d) respectively. Vertical axis is normalised conductance  $g(B)/g(0)$  plotted against logarithmic  $B$  scale. Insets: logarithmic conductance  $1 - g(B)/g(0)$  plotted against logarithmic  $B$ , following the quadratic relation in equation (22).

## Proximity of the second subband to the first subband

In the main text we discuss the absence of a spin gap minima on the first 1D hole conductance plateau for the traces shown in **Figures 1f-g** and **Supplementary Figure 1a,c,e** with reference to the transconductance colour maps in **Figure 4**. Here we directly compare the calculated conductance with the measured conductance for both electrons and holes as a function of scaled gate voltage  $V_g/\Omega_x$  in **Supplementary Figure 5**.

The calculated conductance is shown for electrons in **Supplementary Figure 5a**, where  $U = 0.1$  and  $R = 0$  for magnetic field  $B = 0$  T and  $B = 4$  T ( $\approx 0.4\Omega_x$ ). The measured conductance for 1D electrons is shown in **Supplementary Figure 5b** for magnetic field  $B = 0$  T and  $B = 4$  T ( $\approx 0.4\Omega_x$ ). The model in **Supplementary Figure 5a** is purely 1D and describes only one subband, while **Supplementary Figure 5b** shows two conductance plateaus over the same energy scale.

Particular care must be taken when comparing the purely 1D model to measured conductance in the case of 1D holes with SOI and 0.7 anomaly. In **Supplementary Figure 5c**, the calculated conductance at  $R = 1.26$  shows the 0.7 anomaly structure (indicated by the green arrow), and the spin gap structure (indicated by the blue arrow) on the first plateau. The first ‘riser’ containing the 0.7 structure extends over a gate range of  $\Delta V_g/\Omega_x \sim 1$ , while the spin gap structure extends over a much further range of  $\Delta V_g/\Omega_x \sim 3$ . We compare the calculated conductance with our (scaled) measured conductance in **Supplementary Figure 5d** and find that the second  $n = 2$  subband riser emerges right where we expect the spin gap conductance minima to occur based on **Supplementary Figure 5c**.

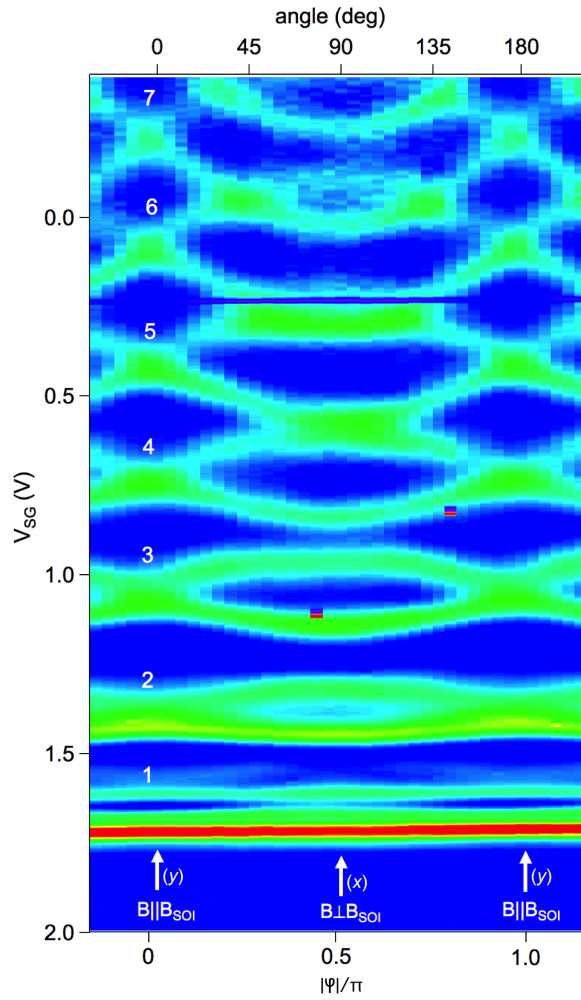


Supplementary Figure 5: (a) Calculated conductance of the first 1D subband for weakly interacting electrons with no SOI. When the magnetic field is increased a half step forms in the conductance trace (red) that crosses the zero-field conductance trace (black). (b) The experimental conductance trace where the spin-resolved conductance trace crosses the zero-field trace similarly to the theoretical model in (a). (c) Calculated conductance of the first 1D subband for strongly interacting holes with strong SOI. The spin-resolved conductance trace (red) does not cross the zero-field trace (black). The 0.7 anomaly is evident at low energy and an emerging dip in the conductance at higher energy is indicative of the opening of the spin gap. (d) The experimental conductance trace where the spin-resolved conductance trace does not cross the zero-field conductance trace, consistent with the theoretical model in (c). The 0.7 anomaly is also evident (indicated by the green arrow). A second shoulder in the conductance above the 0.7 anomaly (indicated by the black arrow) suggests the weak emergence of a dip in conductance due to the opening of the spin gap.



### Anisotropy of the in-plane hole $g$ -factor

In the main text we make note that the anisotropy of the first 1D hole subband ‘splitting’ (that is, the ‘size’ of the 0.7 anomaly in gate voltage (energy)), has the opposite anisotropy to the Zeeman spin-splitting of the higher 1D hole subbands. In **Supplementary Figure 6** we present for the reader’s verification the complete transconductance colour map of  $n = 1..7$  subbands as a function of magnetic field angle with respect to the spin-orbit field  $B_{SOI}$  (or QPC channel). The first subband has a broad (in  $V_{SG}$ ) 0.7 anomaly at  $\varphi/\pi = 0, 1.0$  (or  $B \parallel B_{SOI}$ ); in contrast subbands  $n = 2..7$  have minimal spin splitting. When  $\varphi/\pi = 0.5$  (or  $B \perp B_{SOI}$ ), the opening of the spin gap coincides with the 0.7 anomaly becoming narrower, while subbands  $n = 2..7$  are Zeeman spin-split.



Supplementary Figure 6: Complete transconductance map (of data presented in **Figure 4** in the main text) plotted against  $V_{SG}$  and magnetic field angle  $\varphi$  (angle in degrees provided on top axis), where  $|B| = 4$  T. Magnetic field orientation with respect to the spin-orbit field  $B_{SOI}$ , and the corresponding  $x, y$ -directions, are indicated at the bottom of the colour map. Subbands are labelled 1..7 in white just above the subband at the point of minimal spin-splitting on the left side of the colour map.

## **Zeeman spin-splitting of the first 1D hole subband in the out-of-plane $z$ -direction**

The theory in Ref [1] assigns the direction of the spin orbit field  $B_{SOI}$  to in-plane perpendicular with the QPC ( $y$ -direction). The field will couple to  $B_{SOI}$  when the applied magnetic field has a component either parallel to the QPC ( $x$ -direction) and/or aligned out of the plane of the 2DHG ( $z$ -direction). In the main text of the paper we examined the first subband in the plane of the 2DHG ( $x, y$ -directions). Here we briefly comment on the first subband in an out-of-plane ( $z$ -direction) field.

The quantisation axis for holes confined to a 2D plane is along the  $z$ -direction; light-hole-heavy-hole (LH-HH) mixing leads to a small in-plane component. The out-of-plane tensor component  $g_{zz}$  has been measured to be in the range of  $5 - 7.2$  <sup>11,12</sup>, consistent with theory <sup>13-15</sup>. (The in-plane  $g$ -factors are an order of magnitude smaller, with  $g_{xx} \approx 0.5$  and  $g_{yy}$  generally too small to resolve in measurements <sup>16</sup>).

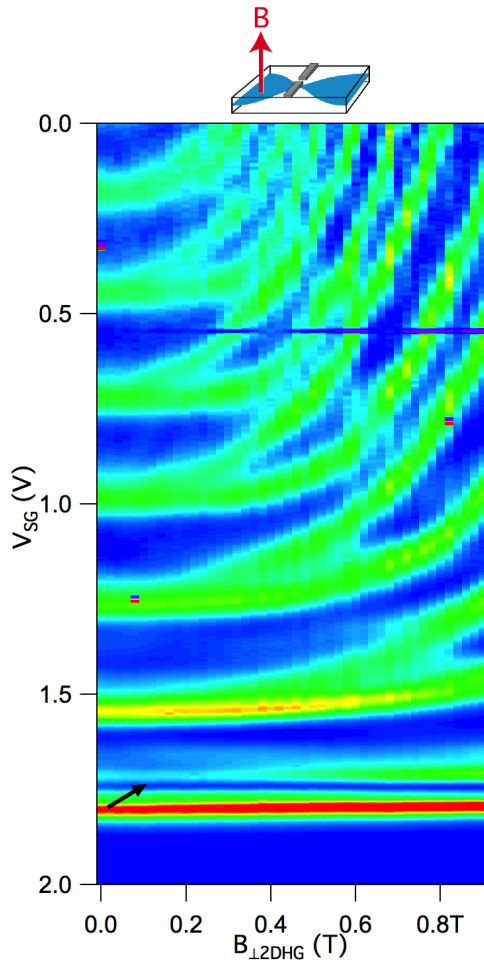
In **Supplementary Figure 7**, the measured transconductance is shown for  $B \perp 2DHG$ , the out-of-plane field direction. At relatively low magnetic field  $B < 1$  T, the large out-of-plane  $g_{zz}$ -factor gives rise to large Zeeman spin-splitting. This field orientation also couples to the orbital momentum of the subbands, resulting in an upward curvature of the subbands. As  $B$  increases, the magnetic length of the holes shrinks and eventually becomes smaller than the width of the 1D constriction, and the higher subbands one by one enter the quantum Hall regime.

When the magnetic field is oriented along the out-of-plane  $z$ -direction, it is also  $B \perp B_{SOI}$

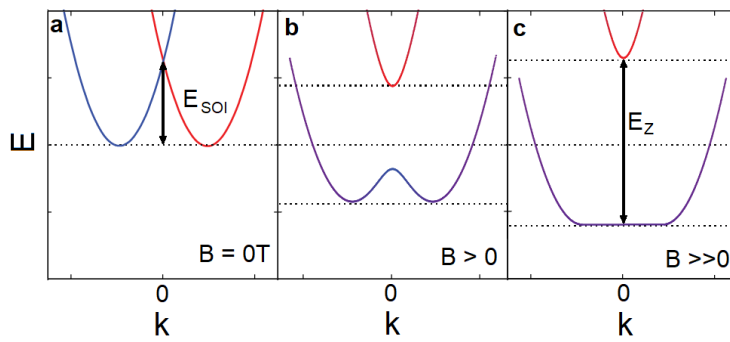
and should open a spin-gap in the first 1D hole subband. This opening of the spin-gap is consistent with the absence of spin-splitting in the first 1D hole subband up to 0.9 T **Supplementary Figure 7**. This behaviour has also been observed in Ref [17] where there is an absence of spin-splitting up to  $\sim 3$  T, and in Ref [11] up to  $\sim 2$  T. At higher field, the first 1D hole subband abruptly begins to spin-split, and the size of the spin-splitting becomes large quickly.

At low magnetic field, the spin-orbit energy  $E_{SOI}$  is larger than the Zeeman energy  $E_Z$ , and the first subband is insensitive to magnetic field. The sudden transition to large spin-splitting occurs when  $E_Z > E_{SOI}$ . In this regime, the spin gap in the dispersion relation has become so large as to resemble the usual parabolic dispersion relation once more, and the bands become sensitive to magnetic field once more (see **Supplementary Figure 8**).

Once the Zeeman energy overwhelms the spin-orbit gap,  $g\mu_B B \gg E_{SOI}$ , we expect the first 1D hole subband to Zeeman spin-split. In our 1D hole QPCs,  $E_{SOI} \approx 500 \mu\text{eV}$  and  $g_{zz} \sim 5$ <sup>12</sup>. We therefore do not expect to observe Zeeman spin-splitting of the first 1D hole subband until  $B > 1.7$  T. This is a higher magnetic field than was accessible in our experiments for this work.



Supplementary Figure 7: Transconductance colour map of Zeeman spin-splitting of the 1D subbands in hole QPC 4 in magnetic field aligned perpendicular to the QPC and out of the 2DHG plane (see schematic above panel). The subbands  $n = 2..6$  strongly spin split in magnetic field, while the first subband in both panels remains unchanged. The position of the 0.7 anomaly is indicated by the black arrows.



Supplementary Figure 8: (a) 1D parabolic dispersion relation spin-split in  $k$  due to SOI. (b) Applied magnetic field results in spin gap opening in 1D dispersion relation at  $k = 0$ .  $E_{SOI} > E_Z$ . (c) Large applied magnetic field results in  $E_Z > E_{SOI}$  and the bands resemble the generic 1D dispersion relation again.

## 4 Fabrication and measurement methods

The following includes information on the device fabrication and electrical set-up for the measurements presented in the Main Text and Supplementary Information.

**Electron QPC device** AuGe was used for the ohmic contacts to the 2DEG. A 20 nm thick layer of  $\text{Al}_2\text{O}_3$  was used to insulate the Ti/Au top gate electrode from the ohmic contacts. Electrical measurements were performed at a temperature of 300 mK using standard AC lock-in techniques with an excitation voltage of  $50 \mu\text{V}$  at a frequency of 7 Hz. QPC electron densities, surface gate dimensions and 2DEG depth are summarised in Supplementary Table 1.

**Hole QPC devices** AuBe was used for the ohmic contacts to the 2DHS. A 20 nm thick layer of  $\text{Al}_2\text{O}_3$  was used to insulate the Ti/Au top gate electrode from the ohmic contacts. Electrical measurements were performed at a temperature of 40 mK using standard AC lock-in techniques with an excitation voltage of  $100 \mu\text{V}$  at a frequency of 7 Hz. QPC hole densities, surface gate dimensions and 2DHG depth are summarised in Supplementary Table 1. QPC 1 has hole mobility of  $\mu = 0.1 \times 10^6 \text{cm}^2 \text{V}^{-1} \text{s}^{-1}$ . QPCs 2-6 have hole mobilities  $\mu = 0.5 \times 10^6 \text{cm}^2 \text{V}^{-1} \text{s}^{-1}$

1. Goulko, O., Bauer, F., Heyder, J. & von Delft, J. Effect of spin-orbit interactions on the 0.7 anomaly in quantum point contacts. *Phys. Rev. Lett.* **113**, 266402 (2014).
2. Datta, S. *Electronic Transport in Mesoscopic Systems* (Cambridge University Press, 1995).
3. Wetterich, C. Exact evolution equation for the effective potential. *Physics Letters B* **301**, 90 – 94 (1993).
4. Birkholz, J. E. & Meden, V. Spin-polarized currents through interacting quantum wires with nonmagnetic leads. *Phys. Rev. B* **79**, 085420 (2009).
5. Birkholz, J. E. *Spin-orbit interaction in quantum dots and quantum wires of correlated electrons – A way to spintronics?* Ph.D. thesis, Georg-August-Universität zu Göttingen (2008).
6. Bauer, F. *0.7 Anomaly of Quantum Point Contacts: Treatment of Interactions with Functional Renormalization Group*. Master's thesis, LMU-München (2008).
7. Metzner, W., Salmhofer, M., Honerkamp, C., Meden, V. & Schönhammer, K. Functional renormalization group approach to correlated fermion systems. *Rev. Mod. Phys.* **84**, 299–352 (2012).
8. Bauer, F., Heyder, J. & von Delft, J. Functional renormalization group approach for inhomogeneous interacting fermi systems. *Phys. Rev. B* **89**, 045128 (2014).
9. Bauer, F. *et al.* Microscopic origin of the ‘0.7-anomaly’ in quantum point contacts. *Nature* **501**, 73–78 (2013).

10. Cronenwett, S. M., Oosterkamp, T. H. & Kouwenhoven, L. P. A tunable Kondo effect in quantum dots. *Science* **281**, 540–544 (1998).
11. Nichele, F. *et al.* Characterization of spin-orbit interactions of GaAs heavy holes using a quantum point contact. *Phys. Rev. Lett.* **113**, 046801 (2014).
12. Srinivasan, A. *et al.* Using a tunable quantum wire to measure the large out-of-plane spin splitting of quasi two-dimensional holes in a GaAs nanostructure. *Nano Letters* **13**, 148–152 (2013).
13. Winkler, R. *Spin-orbit coupling effects in two-dimensional electron and hole systems*. Springer tracts in modern physics (Springer, Berlin, 2003).
14. Zülicke, U. Electronic and spin properties of hole point contacts. *physica status solidi c* **3**, 4354–4358 (2006).
15. Simion, G. E. & Lyanda-Geller, Y. B. Magnetic field spectral crossings of Luttinger holes in quantum wells. *Phys. Rev. B* **90** (2014).
16. Chen, J. C. H. *et al.* Observation of orientation- and  $k$  -dependent Zeeman spin-splitting in hole quantum wires on (100)-oriented AlGaAs/GaAs heterostructures. *New Journal of Physics* **12**, 033043 (2010).
17. Komijani, Y. *et al.* Anisotropic Zeeman shift in p-type GaAs quantum point contacts. *EPL (Europhysics Letters)* **102**, 37002 (2013).